

P- and N-type diluted magnetic semiconductors with narrow band gaps

Bo Gu^{1*} and Sadamichi Maekawa^{1,2}

¹ Advanced Science Research Center, Japan Atomic Energy Agency, Tokai 319-1195, Japan

² ERATO, Japan Science and Technology Agency, Sendai 980-8577, Japan

(Dated: December 3, 2024)

We propose a method to realize diluted magnetic semiconductors (DMS) with p- and n-type carriers by choosing host semiconductors with a narrow band gap. By employing a combination of the density function theory and quantum Monte Carlo simulation, we demonstrate such semiconductors using Mn-doped BaZn₂As₂, which has a band gap of 0.2 eV. In addition, we found a new non-toxic DMS Mn-doped BaZn₂Sb₂, of which the Curie temperature T_c is predicted to be higher than that of Mn-doped BaZn₂As₂, the T_c of which was up to 230 K in the recent experiment.

PACS numbers: 75.50.Pp, 75.30.Hx, 02.70.Ss

After the discovery of ferromagnetism in (Ga,Mn)As, diluted magnetic semiconductors (DMS) have received considerable attention owing to potential applications based on the use of both their charge and spin degrees of freedom in electronic devices [1, 2]. Thus far, the highest Curie temperature of (Ga,Mn)As has been $T_c = 190$ K [3]. The substitution of divalent Mn atoms into trivalent Ga sites introduces hole carriers; thus, (Ga,Mn)As is a p-type DMS. The valence mismatch between Mn and Ga leads to severely limited chemical solubility for Mn in GaAs. Moreover, owing to simultaneous doping of charge and spin induced by Mn substitution, it is difficult to individually optimize charge and spin densities.

To overcome these difficulties, a new type of DMS, i.e., Li(Zn,Mn)As was proposed [4] and later fabricated with $T_c = 50$ K [5]. It is based on LiZnAs, a I–II–V semiconductor. Spin is introduced by isovalent (Zn^{2+} , Mn^{2+}) substitution, which is decoupled from carrier doping with excess/deficient Li concentration. Although Li(Zn,Mn)As was proposed as a promising n-type DMS with excess Li^+ , p-type carriers were obtained in the experiment with excess Li. The introduction of holes was presumably because of the excess Li^+ in substitutional Zn^{2+} sites [5]. Later, another I–II–V DMS, i.e., Li(Zn,Mn)P was reported in an experiment with $T_c = 34$ K [6]. Li(Zn,Mn)P with excess Li was determined to be of p-type as well in the experiment. According to first-principles calculations, the reason for this is the same as that for Li(Zn,Mn)As [6]. Although such p-type I–II–V DMSs have a few distinct advantages over (Ga,Mn)As, the achievable T_c is much lower than that of (Ga,Mn)As.

Another type of DMS $(\text{Ba,K})(\text{Zn,Mn})_2\text{As}_2$ was observed in experiments with T_c up to 230 K [7, 8], which is higher than that for (Ga,Mn)As. Based on the semiconductor BaZn₂As₂, holes were doped by (Ba^{2+} , K^+) substitutions, and spins by isovalent (Zn^{2+} , Mn^{2+}) substitutions. It was a p-type DMS. Motivated by the high T_c , density functional theory (DFT) calculations [9] and photoemission spectroscopy experiments [10, 11] were con-

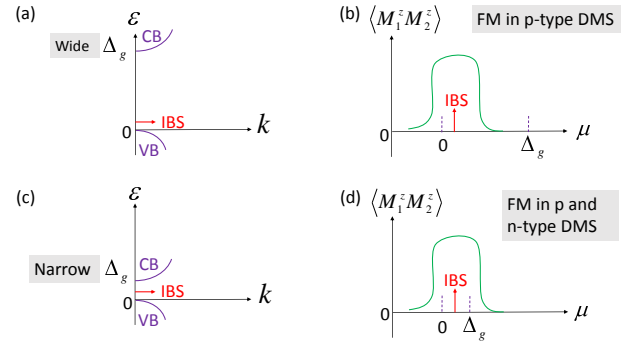


FIG. 1. (Color online) Schematic pictures of impurity bound state (IBS) and ferromagnetic (FM) coupling in diluted magnetic semiconductors (DMS). (a) Host bands $\epsilon(k)$ with a wide band gap Δ_g between the valence band (VB) and the conduction band (CB). The position of the IBS ω_{IBS} (arrow) is close to the top of the VB owing to strong mixing between the impurity and the VB, and usually no IBS appears below the bottom of the CB because of weak mixing between the impurity and the CB [13–15]. We have $0 \lesssim \omega_{\text{IBS}} \ll \Delta_g$. (b) Magnetic correlation $\langle M_1^z M_2^z \rangle$ between two impurities as a function of the chemical potential μ for case (a). Positive $\langle M_1^z M_2^z \rangle$ denotes FM coupling, which can be developed when $\mu \sim \omega_{\text{IBS}}$ [16–18]. Hence, for p-type carriers ($\mu \sim 0$), FM coupling can be obtained as $\mu \sim \omega_{\text{IBS}}$, and for n-type carriers ($\mu \sim \Delta_g$), no magnetic coupling is obtained between impurities because $\mu \gg \omega_{\text{IBS}}$ [13–15]. (c) Similar to case (a), except for a narrow Δ_g . By choosing suitable host semiconductors and impurities, the condition $0 \lesssim \omega_{\text{IBS}} \lesssim \Delta_g$ is obtained. (d) Similar to case (b), except for a narrow Δ_g . FM coupling can be achieved for both p-type and n-type carriers when $\mu \sim \omega_{\text{IBS}}$. In this study, we describe cases (c) and (d).

ducted to understand the microscopic mechanism of ferromagnetism of p-type DMS $(\text{Ba,K})(\text{Zn,Mn})_2\text{As}_2$. By contrast, an n-type DMS, i.e., $\text{Ba}(\text{Zn,Mn,Co})_2\text{As}_2$ was recently reported in an experiment with $T_c \sim 80$ K [12]. In this material, electrons are doped because of the substitution of Zn with Co, and spins are generated mainly because of (Zn^{2+} , Mn^{2+}) substitutions.

In Mn-doped BaZn₂As₂, why is the ferromagnetic (FM) coupling observed in both p- and n-type cases?

* Corresponding author: gu.bo@jaea.go.jp

Why is T_c much lower in the n-type case than that in p-type case? In general, can p- and n-type DMS be realized? The answers will be helpful for fabricating spin p-n junctions in the future. In this study, we attempt to address such issues. In previous studies on DMS materials with wide band gap Δ_g , we found that the position of the IBS ω_{IBS} was close to the top of the VB owing to the strong mixing between the impurity and the VB, and usually no IBS appeared below the bottom of the CB because of weak mixing between the impurity and the CB [13–15]. Thus, we have $0 \lesssim \omega_{\text{IBS}} \ll \Delta_g$, as shown in Fig. 1(a). The magnetic correlation $\langle M_1^z M_2^z \rangle$ between two impurities with FM coupling (positive $\langle M_1^z M_2^z \rangle$) can be determined when the chemical potential μ is tuned to be close to the IBS: $\mu \sim \omega_{\text{IBS}}$ [16–18]. Therefore, for p-type carriers ($\mu \sim 0$), FM coupling can be obtained as $\mu \sim \omega_{\text{IBS}}$, and for n-type carriers ($\mu \sim \Delta_g$), no magnetic coupling is obtained between impurities because $\mu \gg \omega_{\text{IBS}}$. A schematic diagram describing p-type DMS materials with a wide band gap, including (Zn,Mn)O [13], (Ga,Mn)As [14], and Mg(O,N) [15], is shown in Fig. 1(b).

Here, we propose a method for realizing p- and n-type DMS. The key is choosing host semiconductors with a narrow band gap Δ_g . By selecting suitable host semiconductors and impurities, the condition $0 \lesssim \omega_{\text{IBS}} \lesssim \Delta_g$ is satisfied, as shown in Fig. 1(c). We show that for both the p-type ($\mu \sim 0$) and the n-type ($\mu \sim \Delta_g$) cases, the condition for developing FM coupling, that is $\mu \sim \omega_{\text{IBS}}$, can be fulfilled, as shown in Fig. 1(d).

In the following, we realistically calculate the electronic and magnetic properties of Mn-doped BaZn_2As_2 DMS, which has narrow band gap Δ_g ($= 0.2$ eV) [7]. We use a combination of the DFT [19, 20] and the Hirsch–Fye quantum Monte Carlo (QMC) simulation [21]. Our combined DFT+QMC method can be used for in-depth treatment of the band structures of materials and strong electron correlations of magnetic impurities on an equal footing; thus, it can be applied for designing new functional semiconductor- [13–15] and metal-based [22–24] materials. The method involves two calculations steps. First, the Haldane–Anderson impurity model [25] is formulated within the local density approximation for determining the host band structure and impurity–host mixing. Second, magnetic correlations of the Haldane–Anderson impurity model at finite temperatures are calculated using the Hirsch–Fye QMC technique [21].

The Haldane–Anderson impurity model is defined as follows:

$$H = \sum_{\mathbf{k}, \alpha, \sigma} [\epsilon_\alpha(\mathbf{k}) - \mu] c_{\mathbf{k}\alpha\sigma}^\dagger c_{\mathbf{k}\alpha\sigma} + \sum_{\mathbf{k}, \alpha, i, \xi, \sigma} (V_{i\xi\mathbf{k}\alpha} d_{i\xi\sigma}^\dagger c_{\mathbf{k}\alpha\sigma} + h.c.) + (\epsilon_d - \mu) \sum_{i, \xi, \sigma} d_{i\xi\sigma}^\dagger d_{i\xi\sigma} + U \sum_{i, \xi} n_{i\xi\uparrow} n_{i\xi\downarrow}, \quad (1)$$

where $c_{\mathbf{k}\alpha\sigma}^\dagger$ ($c_{\mathbf{k}\alpha\sigma}$) is the creation (annihilation) operator for a host electron with wave vector \mathbf{k} and spin σ in the VB ($\alpha = v$) or the CB ($\alpha = c$), and $d_{i\xi\sigma}^\dagger$ ($d_{i\xi\sigma}$) is

the creation (annihilation) operator for a localized electron at impurity site i in orbital ξ and spin σ with $n_{i\xi\sigma} = d_{i\xi\sigma}^\dagger d_{i\xi\sigma}$. Here, $\epsilon_\alpha(\mathbf{k})$ is the host band dispersion, μ is the chemical potential, $V_{i\xi\mathbf{k}\alpha}$ denotes mixing between the impurity and the host, ϵ_d is the impurity 3d orbital energy, and U is the on-site Coulomb repulsion of the impurity. For simplicity, we neglect Hund coupling.

The parameters $\epsilon_\alpha(\mathbf{k})$ and $V_{i\xi\mathbf{k}\alpha}$ are obtained by DFT calculations using the Wien2k package [26], the details of which are shown in the Supplemental Material [27]. The parameters U and ϵ_d are determined as follows. For (Ga,Mn)As, the reasonable parameters are estimated as $U = 4$ eV and $\epsilon_d = -2$ eV [14]. A recent resonance photoemission spectroscopy experiment showed that the Mn 3d partial density of states in (Ba,K)(Zn,Mn) $_2\text{As}_2$ and (Ga,Mn)As are quite similar, excepted that the peak of (Ga,Mn)As is approximately 0.4 eV deeper than that of (Ba,K)(Zn,Mn) $_2\text{As}_2$ [10]. Thus, the reasonable parameters of Mn-doped BaZn_2As_2 are $U = 4$ eV and $\epsilon_d = -1.5$ eV. On the basis of the parameters obtained above, magnetic correlations of the impurities are calculated using the Hirsch–Fye QMC technique with more than 10^6 Monte Carlo sweeps and a Matsubara time step $\Delta\tau = 0.25$.

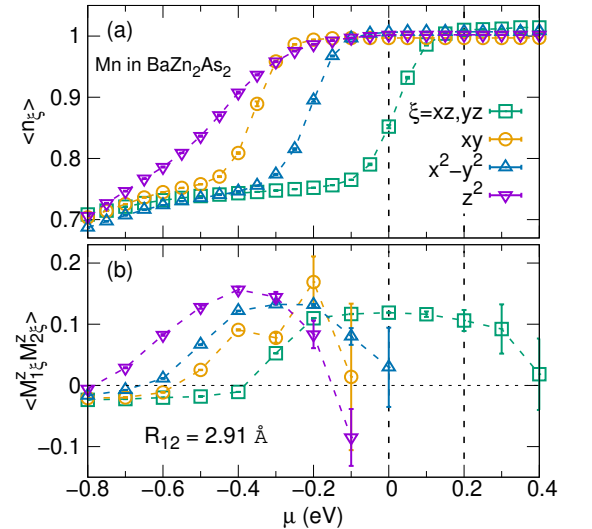


FIG. 2. (Color online) For Mn-doped BaZn_2As_2 , chemical potential μ dependence of (a) occupation number $\langle n_\xi \rangle$ of ξ orbital of an Mn impurity, and (b) magnetic correlation $\langle M_{1\xi}^z M_{2\xi}^z \rangle$ between the ξ orbitals of two Mn impurities with fixed distance $R_{12} = 2.91$ Å (the 1st nearest neighbor), where the temperature is 360 K. The top of the VB was taken to be 0, and the bottom of the CB to be 0.2 eV.

Figure 2 (a) shows a plot of the occupation number $\langle n_\xi \rangle$ of a ξ orbital of an Mn impurity in BaZn_2As_2 against the chemical potential μ at 360 K. The top of the VB was taken to be 0, and the bottom of the CB to be 0.2 eV.

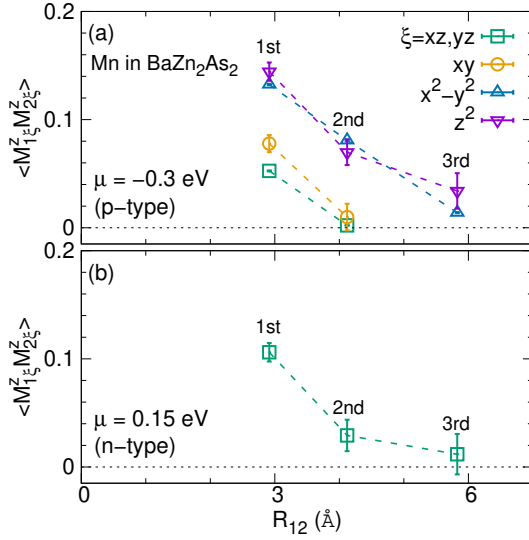


FIG. 3. (Color online) For Mn-doped BaZn₂As₂, the distance R_{12} dependence of magnetic correlation $\langle M_{1\xi}^z M_{2\xi}^z \rangle$ between the ξ orbitals of two Mn impurities for (a) p-type case with chemical potential $\mu = -0.3$ eV and (b) n-type case with $\mu = 0.15$ eV, where temperature is 360 K. The 1st, 2nd, and 3rd nearest neighbors of R_{12} are noted.

Operator n_{ξ} is defined as follows:

$$n_{\xi} = n_{i\xi\uparrow} + n_{i\xi\downarrow}. \quad (2)$$

The orbitals xz and yz of Mn substitutional impurities at the Zn site degenerate owing to the crystal field of BaZn₂As₂, which has a group space of I4/mmm [7]. Sharp increases in n_{ξ} are observed around -0.5 and -0.4 and -0.2 and 0.0 eV for the orbitals $\xi = z^2$ and xy and $x^2 - y^2$ and $xz(yz)$, respectively. This implies the existence of an IBS at this energy ω_{IBS} [13–18]. Figure 2 (b) shows the magnetic correlation $\langle M_{1\xi}^z M_{2\xi}^z \rangle$ between the ξ orbitals of two Mn impurities with fixed distance $R_{12} = 2.91$ Å (the 1st nearest neighbor). The operator $M_{i\xi}^z$ of the ξ orbital at impurity site i is defined as follows:

$$M_{i\xi}^z = n_{i\xi\uparrow} - n_{i\xi\downarrow}. \quad (3)$$

For each ξ orbital, FM coupling is obtained when the chemical potential μ is close to the IBS position, and FM correlations become weaker and eventually disappear when μ moves away from the IBS. This role of the IBS in determining the strength of FM correlations between impurities is consistent with the Hartree–Fock and QMC results of various DMS systems [13–18].

For Mn-doped BaZn₂As₂ with p-type carriers, a recent angle-resolved photoemission spectroscopy (ARPES) experiment showed that the Fermi level (μ) is below the top of the VB by several tenths of an eV and a non-dispersive Mn 3d impurity band is present slightly below the Fermi level [11]. On the basis of the results in Fig. 2 (a), we

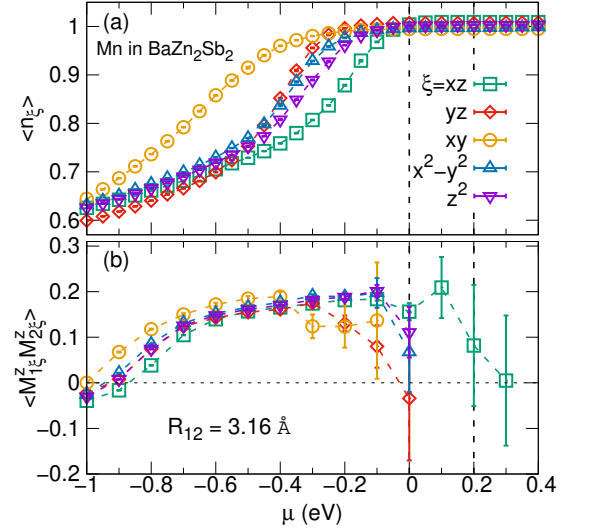


FIG. 4. (Color online) Similar to Fig. 2, except BaZn₂As₂ is replaced by BaZn₂Sb₂.

take $\mu = -0.3$ eV as an estimate for the p-type case. We argue that the IBS of orbitals xy and z^2 , whose positions are below the $\mu = -0.3$ eV, can account for the non-dispersive Mn 3d impurity band below the Fermi level observed in the ARPES experiment. Figure 3 (a) shows the distance R_{12} dependence of the magnetic correlation $\langle M_{1\xi}^z M_{2\xi}^z \rangle$ between the ξ orbitals of two Mn impurities for the p-type case with $\mu = -0.3$ eV. Long-range FM coupling up to approximately 6 Å (the 3rd nearest neighbor) is obtained for the orbitals $\xi = x^2 - y^2$ and z^2 , while short-range FM coupling is obtained for the other three orbitals. Considering Hund coupling, which was ignored in the calculations for simplicity, all five 3d orbitals of the Mn impurity can have long-range FM coupling. Thus, our theoretical results are consistent with the FM observed in the experiment involving Mn-doped BaZn₂As₂ with p-type carriers.

For Mn-doped BaZn₂As₂ with n-type carriers, a recent experiment showed FM coupling below $T_c = 80$ K [12]. Because no information about the Fermi level has been reported, we take $\mu = 0.15$ eV as an estimate for the n-type case, which is below the bottom of the CB by 0.05 eV. As shown in Fig. 3 (b), long-range FM coupling up to approximately 6 Å (the 3rd nearest neighbor) is obtained for the orbitals $\xi = xz$ and yz . No FM is obtained for the other three orbitals, shown in Fig. 2 (b) as well. Considering Hund coupling, as mentioned above, all five 3d orbitals of the Mn impurity can have long-range FM coupling. A Comparison of Figs. 2 (a) and (b) shows that the magnitude of FM coupling $\langle M_{1\xi}^z M_{2\xi}^z \rangle$ in the n-type case is smaller than that in the p-type case, which can qualitatively explain why the T_c in the n-type case [12] is lower than that in the p-type case [7, 8] in the experiments.

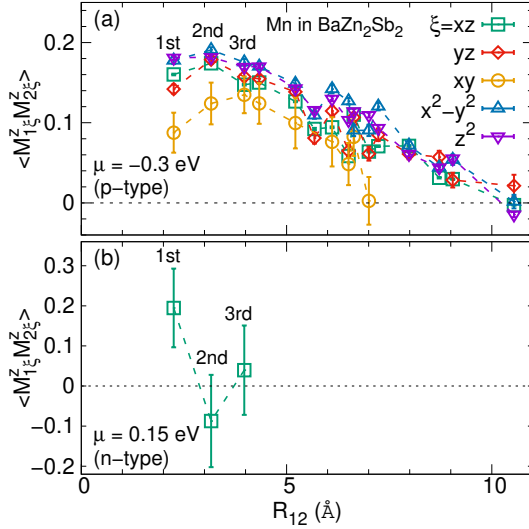


FIG. 5. (Color online) Similar to Fig. 3, except BaZn₂As₂ is replaced by BaZn₂Sb₂.

We made similar calculations for Mn-doped BaZn₂Sb₂, where a distinct advantage was the replacement of As with non-toxic Sb. BaZn₂Sb₂, too, has a narrow band gap $\Delta_g = 0.2$ eV, but a different space group Pnma [28]. Figure 4 (a) shows the occupation number $\langle n_\xi \rangle$ of the ξ orbital of the Mn impurity in BaZn₂Sb₂ versus chemical potential μ at temperature 360 K. The 3d orbitals of Mn did not degenerate owing to the low symmetry of the crystal field of BaZn₂Sb₂. Sharp increases in $\langle n_\xi \rangle$, which imply the position of IBS ω_{IBS} , were observed around -0.6 eV for the xy orbital, -0.4 eV for the yz and $x^2 - y^2$ and z^2 orbitals, and -0.2 eV for the xz orbital. Figure 4 (b) shows the magnetic correlation $\langle M_{1\xi}^z M_{2\xi}^z \rangle$ between the ξ orbitals of two Mn impurities with fixed distance $R_{12} = 3.16$ Å (the 2nd nearest neighbor). The role of the IBS in determining the strength of the FM correlations between impurities is the same as discussed for Mn-doped BaZn₂As₂ in Fig. 2.

For Mn-doped BaZn₂Sb₂ with p-type carriers, we take

$\mu = -0.3$ eV, the same value as that used for Mn-doped BaZn₂As₂ with p-type carriers. Figure 5 (a) shows the distance R_{12} dependence of the magnetic correlation $\langle M_{1\xi}^z M_{2\xi}^z \rangle$ between the ξ orbitals of two Mn impurities for the p-type case. Long-range FM coupling up to approximately 10 Å (the 14th nearest neighbor) was obtained for the $\xi = xz, yz, x^2 - y^2$ and z^2 orbitals, while relatively short-range FM coupling is obtained for the xy orbital. Considering Hund coupling, which is ignored in the calculations, all five 3d orbitals of the Mn impurity can have long-range FM coupling up to approximately 10 Å (the 14th nearest neighbor). This is considerably longer than 6 Å (the 3rd nearest neighbor) obtained for Mn doped BaZn₂As₂ with p-type carriers, as shown in Fig. 3 (a). Such long-range FM coupling arises from the short distance between the neighboring Zn sites in BaZn₂Sb₂, as is clear from comparison of the 1st and 2nd and 3rd nearest neighbors in Fig. 3(a) and those neighbors in Fig. 5(a), respectively. We predict that the T_c of Mn-doped BaZn₂Sb₂ with p-type carriers should be higher than that of Mn-doped BaZn₂As₂ with p-type carriers, in which $T_c = 230$ K was reported in a recent experiment [8].

For Mn-doped BaZn₂Sb₂ with n-type carriers, we take $\mu = 0.15$ eV, the same value as that used for Mn-doped BaZn₂As₂ with n-type carriers. As shown in Fig. 5 (b), no stable magnetic couplings were obtained for the 2nd and 3rd nearest neighbors owing to large error bars; thus, there was no long-range FM coupling. This is because $\mu = 0.15$ eV is slightly far from the IBS position of the xz orbital, which is approximately -0.2 eV, as shown in Fig. 4 (a).

In summary, we have proposed a method to realize DMS with p- and n-type carriers by choosing host semiconductors with a narrow band gap. Using the combined method of DFT and QMC, we describe DMS Mn-doped BaZn₂As₂, which has a narrow band gap of 0.2 eV. In addition, we find a new non-toxic DMS Mn-doped BaZn₂Sb₂, whose T_c is expected to be higher than that of Mn-doped BaZn₂As₂, for which $T_c = 230$ K, as reported in a recent experiment.

The authors acknowledge H. Y. Man, F. L. Ning, C. Q. Jin, H. Suzuki, and A. Fujimori for many valuable discussions about the experiments of Mn-doped BaZn₂As₂.

- [1] H. Ohno, Science **281**, 951 (1998).
- [2] T. Dietl, Nat. Mater. **9**, 965 (2010).
- [3] M. Wang, R. P. Campion, A. W. Rushforth, K. W. Edmonds, C. T. Foxon, and B. L. Gallagher, Appl. Phys. Lett. **93**, 132103 (2008).
- [4] J. Masek, J. Kudrnovsky, F. Maca, B. L. Gallagher, R. P. Campion, D. H. Gregory, and T. Jungwirth, Phys. Rev. Lett. **98**, 067202 (2007).
- [5] Z. Deng, C. Q. Jin, Q. Q. Liu, X. C. Wang, J. L. Zhu, S. M. Feng, L. C. Chen, R. C. Yu, C. Arguello, T. Goko, F. Ning, J. Zhang, Y. Wang, A. A. Aczel, T. Munsie, T.

- J. Williams, G. M. Luke, T. Kakeshita, S. Uchida, W. Higemoto, T. U. Ito, B. Gu, S. Maekawa, G. D. Morris, and Y. J. Uemura, Nat. Commun. **2**, 422 (2011).
- [6] Z. Deng, K. Zhao, B. Gu, W. Han, J. L. Zhu, X. C. Wang, X. Li, Q. Q. Liu, R. C. Yu, T. Goko, B. Frandsen, L. Liu, J. Zhang, Y. Wang, F. L. Ning, S. Maekawa, Y. J. Uemura, and C. Q. Jin, Phys. Rev. B **88**, 081203(R) (2013).
- [7] K. Zhao, Z. Deng, X. C. Wang, W. Han, J. L. Zhu, X. Li, Q. Q. Liu, R. C. Yu, T. Goko, B. Frandsen, L. Liu, F. L. Ning, Y. J. Uemura, H. Dabkowska, G. M. Luke, H.

- Luetkens, E. Morenzoni, S. R. Dunsiger, A. Senyshyn, P. Boni, and C. Q. Jin, *Nat. Commun.* **4**, 1442 (2013).
- [8] K. Zhao, B. J. Chen, G. Q. Zhao, Z. Yuan, Q. Q. Liu, Z. Deng, J. L. Zhu, and C. Q. Jin, *Chin. Sci. Bull.* **59**, 2524 (2014).
- [9] J. K. Glasbrenner, I. Zutic, and I. I. Mazin, *Phys. Rev. B* **90**, 140403(R) (2014).
- [10] H. Suzuki, K. Zhao, G. Shibata, Y. Takahashi, S. Sakamoto, K. Yoshimatsu, B. J. Chen, H. Kumigashira, F. H. Chang, H. J. Lin, D. J. Huang, C. T. Chen, B. Gu, S. Maekawa, Y. J. Uemura, C. Q. Jin, and A. Fujimori, *Phys. Rev. B* **91**, 140401(R) (2015).
- [11] H. Suzuki, G. Q. Zhao, K. Zhao, B. J. Chen, M. Horio, K. Koshiishi, J. Xu, M. Kobayashi, M. Minohara, E. Sakai, K. Horiba, H. Kumigashira, B. Gu, S. Maekawa, Y. J. Uemura, C. Q. Jin, and A. Fujimori, *Phys. Rev. B* **92**, 235120 (2015).
- [12] H. Y. Man, C. Ding, S. L. Guo, G. X. Zhi, X. Gong, Q. Wang, H. D. Wang, B. Chen, and F. L. Ning, *arXiv:1403.4019* (unpublished).
- [13] B. Gu, N. Bulut, and S. Maekawa, *J. Appl. Phys.* **104**, 103906 (2008).
- [14] J. Ohe, Y. Tomoda, N. Bulut, R. Arita, K. Nakamura, and S. Maekawa, *J. Phys. Soc. Jpn.* **78**, 083703 (2009).
- [15] B. Gu, N. Bulut, T. Ziman, and S. Maekawa, *Phys. Rev. B* **79**, 024407 (2009).
- [16] M. Ichimura, K. Tanikawa, S. Takahashi, G. Baskaran, and S. Maekawa, *Foundations of Quantum Mechanics in the Light of New Technology*, edited by S. Ishioka and K. Fujikawa. (World Scientific, Singapore, 2006), pp. 183-186.
- [17] N. Bulut, K. Tanikawa, S. Takahashi, and S. Maekawa, *Phys. Rev. B* **76**, 045220 (2007).
- [18] Y. Tomoda, N. Bulut, and S. Maekawa, *Physica B* **404**, 1159 (2009).
- [19] P. Hohenberg and W. Kohn, *Phys. Rev.* **136**, B864 (1964).
- [20] W. Kohn and L. J. Sham, *Phys. Rev.* **140**, A1133 (1965).
- [21] J. E. Hirsch and R. M. Fye, *Phys. Rev. Lett.* **56**, 2521 (1986).
- [22] B. Gu, J. Y. Gan, N. Bulut, T. Ziman, G. Y. Guo, N. Nagaosa, and S. Maekawa, *Phys. Rev. Lett.* **105**, 086401 (2010).
- [23] B. Gu, I. Sugai, T. Ziman, G. Y. Guo, N. Nagaosa, T. Seki, K. Takanashi, and S. Maekawa, *Phys. Rev. Lett.* **105**, 216401 (2010).
- [24] Z. Xu, B. Gu, M. Mori, T. Ziman, and S. Maekawa, *Phys. Rev. Lett.* **114**, 017202 (2015).
- [25] F. D. M. Haldane and P. W. Anderson, *Phys. Rev. B* **13**, 2553 (1976).
- [26] P. Blaha, K. Schwartz, G. K. H. Hadsen, D. Kvasnicka, and J. Luitz, WIEN2K, An Augmented Plane Wave Plus Local Orbitals Program for Calculating Crystal Properties, Vienna University of Technology, Vienna, 2001.
- [27] See Supplemental Material for DFT calculations on the parameters of host band and mixing.
- [28] G. K. H. Madsen, *J. Am. Chem. Soc.* **128**, 12140 (2006).